



Linkage between the absorbing aerosol-induced snow darkening effects over the Himalayas-Tibetan Plateau and the pre-monsoon climate over northern India

Sushant Das¹ · Filippo Giorgi¹ · Erika Coppola¹ · A. S. Panicker² · A. S. Gautam³ · Vijayakumar S. Nair⁴ · Graziano Giuliani¹

Received: 25 May 2021 / Accepted: 13 November 2021 / Published online: 26 November 2021
© The Author(s), under exclusive licence to Springer-Verlag GmbH Austria, part of Springer Nature 2021

Abstract

The role of aerosol on the snow darkening effect is considered one of the main factors contributing to snow melting and glacier retreat over the Himalayas and Tibetan Plateau (HTP). Using the International Centre for Theoretical Physics (ICTP)'s regional climate model, RegCM4, we examine the changes induced by aerosol deposition over the HTP snow and its dynamical impacts over northern India during the pre-monsoon season (March to June), which is critical for the inception and development of the monsoon. Sensitivity experiments with and without aerosol-induced snow darkening effects for the period 2006–2010 reveal that this effect causes a significant reduction of snow cover fraction by 10 to 15% and an increase in surface temperatures (> 4 °C), which improves the model performance when comparing against observations over the HTP. This response is dominated by dust deposition, which covers a larger area of the HTP compared to the black carbon. While incorporating aerosol-induced snow darkening effect, the precipitation decreases (~ 0.4 – 2 mm/day) over northern India due to intrusion of dry winds, which also enhance dust emissions over the Thar Desert. As a result of the decrease in precipitation, surface temperature increases and generates a low-pressure system over northern India, which further strengthens the dust transport and its burden. We also find decreases in precipitation extremes and increases in the number of consecutive dry days and extreme temperature conditions over northern India, implying strong links with changes in pre-monsoon dynamics. The aerosol-induced snow darkening effect thus facilitates an earlier monsoon onset over southern India, but the northward propagation of the precipitation band is limited by the enhanced northwesterly winds over the Indo-Gangetic Plain.

1 Introduction

Aerosols can affect climate directly due to their absorption and scattering of radiation, and indirectly by changing the cloud microphysical properties (e.g., Twomey 1974; Albrecht 1989; Giorgi et al., 2002; Wang 2013; Bond et al., 2013; Fan et al., 2016). Many studies have been carried out to assess the aerosol climatic effects from local to global scales and, depending upon season, different types of aerosols can

affect temperature, circulations, and precipitation (e.g., Ramanathan et al., 2005, Lau et al., 2006, Bollasina et al., 2011, Kumar et al., 2014, Panicker et al., 2010, Bond et al., 2013, Li et al., 2016, Guo et al., 2016, Das et al., 2020a, Ojha et al., 2020). In particular, aerosol-cryosphere interactions (Dagsson-Waldhauserova and Meinander, 2019) and related climatic impacts is a topic of current scientific interest, although not extensively studied in the literature (e.g., Flanner et al., 2009; He et al., 2017; Ming et al., 2013; Lee et al., 2017; Lau and Kim 2018). Absorbing aerosol deposition on snow can modulate the regional water balance by changing the physical properties of snow packs (e.g., snow albedo, snowmelt etc.), for example, increasing snow melt close to high dust and anthropogenic aerosol emission sources (Schmale et al., 2017; Ji et al., 2015).

The Himalayas-Tibetan Plateau (HTP), also widely known as the ‘third pole’ region, is characterized by large amounts of fresh snow packs. The HTP is located between two highly polluted regions, namely East and South Asia,

✉ Sushant Das
sdas@ictp.it; sushant857@yahoo.co.in

¹ Earth System Physics Section, The Abdus Salam International Centre for Theoretical Physics, Trieste, Italy

² Indian Institute of Tropical Meteorology, Pune, India

³ HNB Garhwal University, Srinagar, Uttarakhand, India

⁴ Space Physics Laboratory, Vikram Sarabhai Space Centre, ISRO, Thiruvananthapuram, India

and is surrounded by important desert dust sources, e.g., the Taklamakan, Gobi, Thar, and west Asian deserts. In addition, dust deposition over the HTP can derive from long-range transport from Africa and Middle East deserts (Hu et al., 2020; Zhang et al., 2015; Kang et al., 2016; Sarangi et al., 2020). Recent studies have shown that the deposition of light-absorbing aerosols such as mineral dust and black carbon over snow can enhance the solar absorption at the surface and thus enhance snowmelt over the HTP, a phenomenon known as snow darkening effect (Ji et al., 2015; Lau and Kim 2018). This phenomenon not only has a large climatic impact at the surface (e.g., albedo, surface heat fluxes) but can also modify the thermal structure of the atmosphere and wind circulation patterns (Das et al., 2020b).

Pre-monsoon (March to June) atmospheric conditions are important in modulating the arrival of the Indian summer monsoon (ISM) season. Studies have indicated a strong relation between the pre-monsoon circulations and the following ISM, e.g., the pre-monsoonal diabatic heating prepares the land region to transit into a regime highly conducive to atmospheric convection during the monsoon onset (Ashfaq et al., 2020). Both the changes in latent and sensible heat flux, with the associated dynamics, contribute to affect such transition from the pre-monsoon to the ISM, and therefore any perturbation to the dynamics of the pre-monsoon season can be important for the ISM onset and development.

During the pre-monsoon season, natural mineral dust constitutes the majority of the total aerosol load over northern India. The dust cycle over the region begins with the emission of dust particles from the surrounding arid and semi-arid regions depending on wind speed and soil moisture characteristics (Zakey et al., 2006). Most dust storms occur during the pre-monsoon season in northern India, causing a substantial degradation in visibility (Dey et al., 2004; Srivastava et al., 2011; Sharma et al., 2012; Sarkar et al., 2018; Dumka et al., 2019). The increase in the dust burden is mostly related to an increase in the westerly winds that carry dust from the Thar Desert towards the Indo-Gangetic Plain (IGP). The intensification of these westerly winds has also been associated with the dust-induced snow darkening effect over the HTP (Shi et al., 2018).

Using the Community Atmosphere Model (CAM), Qian et al. (2011) reported a positive warming over the HTP induced by reduced snow albedo due to aerosol deposition. Similar warming and acceleration of snowmelt were reported using the NASA-GEOS-5 model by Yasunari et al. (2014). Lau and Kim (2006) proposed the 'Elevated Heat Pump (HTP)' mechanism, by which the radiative heating induced by the atmospheric aerosols during the pre-monsoon along the Himalayan foothills can affect the Indian monsoon onset and circulation features over India. However, in these studies, the experiments were conducted with coarse resolution models, which may not capture well the dynamical

processes involved and the effect of the steep topographical features of the region.

More recently, RCMs have been used to carry out experiments including the aerosol snow darkening effects over the HTP (e.g., Sarangi et al., 2018; Usha et al., 2020; Das et al., 2020b). From these studies, it is evident that RCMs have good potential to simulate more realistic changes in snow cover and melting due to the aerosol deposition, along with the corresponding atmospheric responses. However, although several RCM studies have examined the effects of aerosol transport (e.g., Nair et al., 2012; Das et al., 2013; Kumar et al., 2014; Ajay et al., 2019) and dust variability (e.g., Aloysius et al., 2011; Kumar et al., 2014) over India, they did not analyze in detail the snow darkening effect on local dynamical features, particularly during the pre-monsoon season.

In general, previous studies have shown that there exist large discrepancies between simulated and observed temperature characteristics over high elevation snow-covered regions such as the HTP. For example, Rana et al. (2020) showed large cold biases over the HTP, up to 5–7 °C, in a set of global and regional climate models (GCMs and RCMs, respectively). Sanjay et al. (2017) also found cold biases of similar magnitude over the HTP in an ensemble of RCM simulations from the Co-ordinated Regional Climate Downscaling Experiment (CORDEX; Giorgi et al. 2009). Although many factors can affect this bias, including possible uncertainties in observations, it is possible that the bias can be at least partially reduced by considering the aerosol-induced snow darkening effect (Ji et al., 2015; Usha et al., 2021).

Based on these considerations, in this paper, we use an RCM including aerosol-induced snow darkening effects to address a number of scientific questions. Does the inclusion of the aerosol-induced snow darkening effect in the model improve the temperature simulation over the HTP? Is there a relation between the snow darkening effect over the HTP and the aerosol distribution in northern India? If so, what are the meteorological variables affected and the underlying changes in the physical processes that modulate the regional aerosol cycle? What is the dynamical effect of snow darkening on the daily characteristics of precipitation and temperature over northern India? All these questions are addressed here, with a focus on the pre-monsoon season, through a series of sensitivity experiments described in the next section. Section 3 then discusses the results of our simulations and Sect. 4 presents our main conclusions.

2 Methodology

2.1 RegCM4, physics, and couplings

We use the Abdus Salam International Centre for Theoretical Physics (ICTP) Regional Climate Model, version 4

(RegCM4, Giorgi et al., 2012), which is a community model used for a wide range of applications (Giorgi et al. 2012; Giorgi, 2019). In particular, RegCM4 has been extensively used over South Asia to study the Indian summer and winter monsoon dynamics and precipitation characteristics (e.g., Pattanayak et al., 2016; Tiwari et al., 2016) along with the cycle and climatic effects of different types of aerosols (e.g., Das et al., 2015, 2020a; Ajay et al., 2019; Maharana et al., 2019).

In brief, RegCM4 is a sigma coordinate model following the hydrostatic approximation. It has a number of physics options that users can select for carrying out their experiments. In our case, we adopted a mixed cumulus parameterization scheme, i.e., Tiedtke (1989) over ocean and MIT (Emanuel and Zivkovic-Rothman, 2000) over land, and the SUBEX scheme (Pal et al., 2000) for resolvable-scale precipitation. The radiation transfer scheme and boundary layer parameterization are represented by Kiehl et al. (1996) and Grenier and Bretherton, (2001), respectively, and land surface processes are described by the community land surface model CLM4.5 (Oleson et al., 2013). This model configuration is the same as used by Das et al. (2020a), and was shown to provide a reasonably good representation of the monsoon climate of South Asia.

For the aerosol cycle, i.e., aerosol emission, transport, and deposition, RegCM4 is coupled with an online aerosol module described by Solmon et al. (2006) and Zakey et al. (2006, 2008), in which both natural and anthropogenic aerosol species are accounted for with specified optical properties (e.g., extinction coefficient, single scattering albedo, and asymmetry parameter). The module includes mineral dust and sea salt as natural components and black carbon (BC), organic carbon (OC), and sulfates as anthropogenic components. For the carbonaceous aerosol species (BC and OC), both hydrophobic and hydrophilic states are considered. When the BC and OC are emitted from the source, they are in the hydrophobic state, and they are converted to the hydrophilic state with an ageing time of ~ 1.15 days (Solmon et al. 2006).

The anthropogenic aerosol species are provided to the model using different emission inventories (see details in the next section). Sea salt particles are generated online depending on the wind stress over the open ocean surface (Zakey et al., 2008). The dust cycle is represented by the Dust Entrainment and Deposition (DEAD) scheme, in which the dust is first generated over arid and semi-arid areas and is then transported through advection and convection and removed through dry and wet deposition processes (Solmon et al. 2006). Dust generation occurs when the near-surface winds are above a given threshold velocity and depends on the properties of the land surface (e.g., soil moisture, vegetation, soil type). More details about the DEAD scheme can be found in Zender et al. (2003).

The RegCM4 coupled with CLM4.5 simulates the fraction of the ground covered by snow based on the method of Swenson and Lawrence (2012). Depending upon the snow depth, the number of snow layers varies and can reach a maximum of five. RegCM4 is also coupled with the Snow, Ice and Aerosol Radiative (SNICAR) module, which is embedded within CLM4.5. The snow albedo is function of the radiative transfer within the snow layers, aerosols, and snow ageing. As the aerosol gets deposited over the snow-covered region, its interaction with the snow occurs through the radiative transfer calculations taking into account the optical properties of the aerosol species and snow grains (Flanner et al., 2007). Currently, the version of SNICAR used in our model configuration considers only the external mixing of aerosol and snow grains. Internal mixing between the aerosol and snow has been recently included in SNICAR (He et al., 2018); however, this is yet to be implemented in RegCM4.

2.2 Domain, boundary conditions, and anthropogenic aerosol emissions

The simulations are carried out over the South Asian CORDEX domain, which includes the HTP and Indian subcontinent (Fig. 1) and has been extensively used in previous studies. The model top is set at 50 hPa and the atmosphere has 23 vertical sigma levels. The horizontal grid point spacing is 50 km, the standard CORDEX resolution, which allows us to carry out different sensitivity experiments with coupled aerosols. The buffer zone consists of 19 grid points along the boundary of the domain.

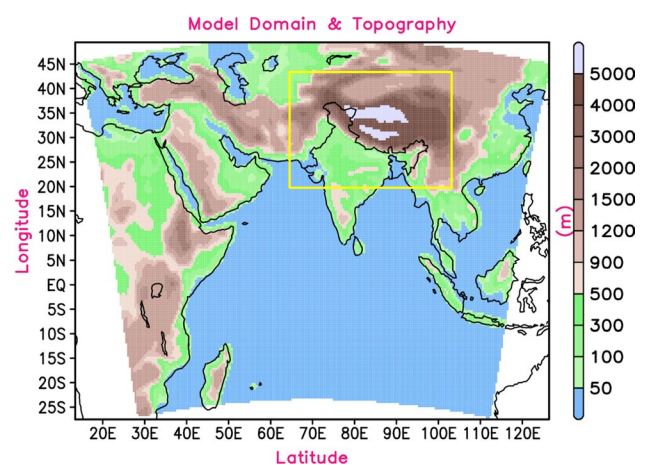


Fig. 1 Model domain considered for carrying out simulations over South Asia CORDEX domain. The shaded colors represent topography at 50-km resolution. The rectangular yellow box is the region of analysis encompassing the Himalayas-Tibetan Plateau (HTP) and northern India

The sea surface temperature (SST) is taken from the National Oceanic and Atmospheric Administration (NOAA) at a resolution of $1^\circ \times 1^\circ$ and the topography, including land use, is from the United States Geological Survey (USGS) at 30-s resolution. The model is driven by six hourly lateral boundary conditions from the EIN15 reanalysis data (Dee et al., 2011) available at a resolution of $1.5^\circ \times 1.5^\circ$. The aerosol boundary conditions are provided from global simulations carried out using the Community Atmosphere Model (CAM) under the Representative Concentration Pathway scenario 2.6 (RCP2.6).

The anthropogenic aerosol emissions of BC and OC are obtained from the Evaluating the Climate and Air Quality Impacts of Short-Lived Pollutants (ECLIPSE) project. More details about the project and its preparation using the Greenhouse gas-Air pollution Interactions and Synergies (GAINS) model can be found in Stohl et al. (2015). The project provides various emission scenarios, e.g., mitigation, baseline, climate, flaring emission, etc., globally based on regulations and each country's government protocols. We use the BC and OC emissions following the current legislature 'baseline scenario' available at a resolution of 50 km. The emissions are mainly from power plants, industrial combustion, agricultural burning fields, residential and commercial, waste management, shipping emissions, and surface transport. Time series of emissions for each species, i.e., BC and OC in our case, are calculated using monthly prescribed weights.

2.3 Experimental designs

We carried out and intercompared two experiments in order to assess the aerosol-induced snow darkening effects over the HTP and its feedbacks over northern India during the pre-monsoon period. In the first experiment, only the direct radiative effects (DRE) of aerosols are considered, while in the second, both the DRE and snow darkening (SD) effects are included ($SDDRE = SD + DRE$). Note that the model does not yet include representation of aerosol indirect effects on cloud microphysics, an implementation that is currently still underway. We ran the model from 1 January 2005 to 31 December 2010 and the analysis is carried out for the 5-year period 2006 to 2010, thus discarding the initial year as a model spin up time. Following Lau and Kim (2018), we only consider light-absorbing aerosols (dust, OC, and BC) in our simulations, thus disregarding the effect of additional particulate matter such as sulfates, nitrates, and secondary organic aerosols. Although OC is included in our experimental setup, its interaction with the snow in the current SNICAR module in RegCM4 is not considered (Flanner et al., 2007).

Previously, Das et al. (2020b) used a similar experimental design to isolate the impacts on regional monsoon dynamics associated with the aerosol direct radiative and

snow darkening effects. Here, we focus more on the pre-monsoon season, which is critical for the development of the monsoon, and on different climate statistics, including the dust cycle and the occurrence of temperature extremes. It is important to note that, according to the India Meteorology Department (IMD), the monsoon normally arrives at around the last week of June or first week of July over north and to northwest India (e.g., 23–24 June at New Delhi and 5–6 July at Bikaner). We, therefore, chose March to June as the pre-monsoon season for our analysis.

2.4 Observation datasets

Here, we consider temperature, precipitation, aerosol optical depth (AOD), and snow fraction, comparing the model results with various observation datasets. Observed mean and maximum near-surface air temperature are obtained from the Climate Research Unit (CRU) dataset version 4.03 at a $0.5^\circ \times 0.5^\circ$ resolution. The CRU monthly gridded data are obtained by using an angular-distance weighting technique starting from extensive networks of weather station observations (Harris et al., 2020). Precipitation data at a resolution of 25 km are from the Tropical Rainfall Measuring Mission (TRMM) version 7 dataset, which is obtained by combining multiple satellite and rain gauge measurements (Huffman et al., 2010). Observed AOD and snow fraction is taken from the Moderate Resolution Imaging Spectrometer (MODIS) sensor onboard the Aqua satellite. Specifically, we use the MODIS Deep Blue aerosol product at a resolution of $1^\circ \times 1^\circ$ and snow fraction data available at 5-km resolution. The MODIS Deep Blue algorithm of Levy et al. (2013) is used to estimate the AOD over bright surfaces such as desert and snow-covered regions. Details of the snow fraction retrieval technique and uncertainties involved are available in Hall and Riggs (2007).

3 Results and discussion

3.1 Model evaluation and aerosol-induced snow darkening effects

We first evaluate mean and maximum near-surface air temperature during the pre-monsoon season. Figure 2 shows that the model in both experiments simulates higher temperatures ($> 32^\circ \text{C}$) over the Thar Desert and IGP compared to CRU ($\sim 28^\circ$ to 32°C). Over the HTP region, the model shows a cold bias, which however is reduced when aerosol-snow interactions are considered (SDDRE). These biases should be viewed within the context of the uncertainties in observations, which can be high in mountainous regions due to the sparsity of stations and, more importantly, the lack of high elevation ones, which would artificially amplify a model

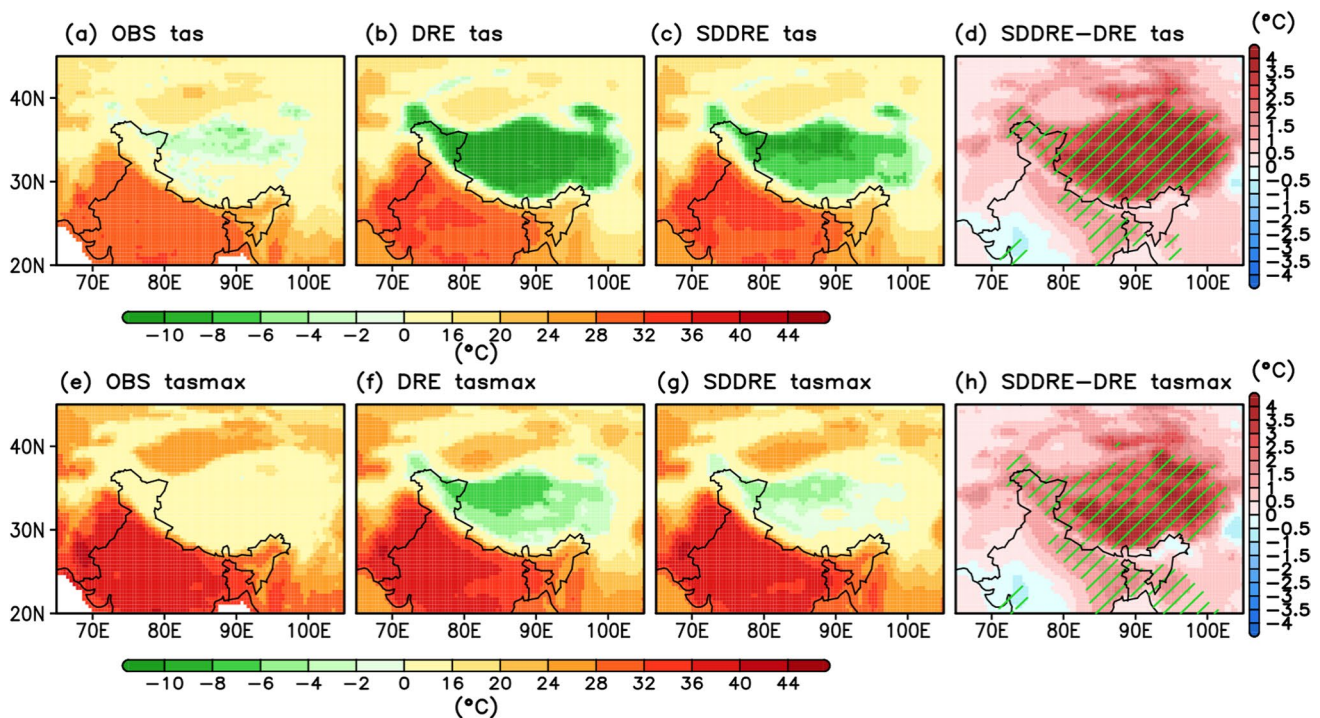


Fig. 2 Spatial distributions of mean near-surface temperature (top panel) from **a** CRU, **b** DRE, **c** SDDRE, and **d** difference between SDDRE and DRE. Similar arrangement in the bottom panel (**e–h**)

for maximum surface temperature during the pre-monsoon (March to June) season for the period 2006–2010. The green slant lines represent regions with 95% significance level

cold bias by overestimating observed regional temperatures. In addition, the imbalance in the surface energy budget can also contribute to such temperature biases over the HTP (Chen and Liu, 2017). Another reason for the cold bias can be attributed to the excessive amounts of simulated snow (discussed later), which is reduced in SDDRE compared to DRE. This effect is more evident during midday when dust and anthropogenic aerosols are emitted more effectively and transported towards the HTP. In fact, when looking at the maximum temperature patterns, the magnitude of the cold bias over the HTP is significantly reduced (>4 °C) in SDDRE compared to DRE (Fig. 2f–g). The bias map also indicates a greater decrease of the mean and maximum temperature bias over the HTP in SDDRE (Figure S1). Also over northern India, the maximum temperatures are closer to observations in SDDRE compared to DRE, implying that some changes in dynamics are at play.

Next, we look into the distribution of AOD (top panel in Fig. 3). Quantitatively, the AOD gradient from high values (>0.6) over the Thar Desert towards the lower values (~ 0.3) in the IGP is seen in both the DRE and SDDRE cases. During the pre-monsoon, desert dust constitutes the main portion of the total aerosol load and frequent dust storms are observed during this season (Dey and Di Girolamo 2010). The model underestimates the AOD over the eastern IGP; however, these regions are affected by other anthropogenic

aerosol species emissions, e.g., sulfates and nitrates from power plants, industries, transportation, and biomass burning, which are not included in our model simulations. It is interesting to note that in SDDRE, there is an increase in AOD over the desert regions, i.e., Thar Desert and Taklamakan Desert (>0.1), and to a lesser extent over the IGP (~ 0.06 – 0.09).

The precipitation patterns also improve over northern India in the SDDRE experiment compared to DRE, being closer to the TRMM observations. In fact, in SDDRE, precipitation decreases over northern India and increases over the HTP, thus exhibiting a dipole response pattern to the snow darkening effect. The large precipitation amounts in the steep mountain slopes can be attributed to the topographical forcings in RegCM4 (Fig. 3f–g). Also for precipitation, however, there can be substantial uncertainties in observations, for example, in the retrieval technique adopted for the TRMM satellites or the effect of a relatively small number of rain gauges over such complex topographical regions (Liu 2015). The increase in precipitation found in SDDRE over the HTP can be at least partially due to the increased snow melting and latent heat fluxes process initiated by the deposition of aerosols (discussed later).

The bottom panel in Fig. 3 shows the observed (MODIS) and simulated snow cover fraction in both experiments. There is a significant reduction of snow fraction over the

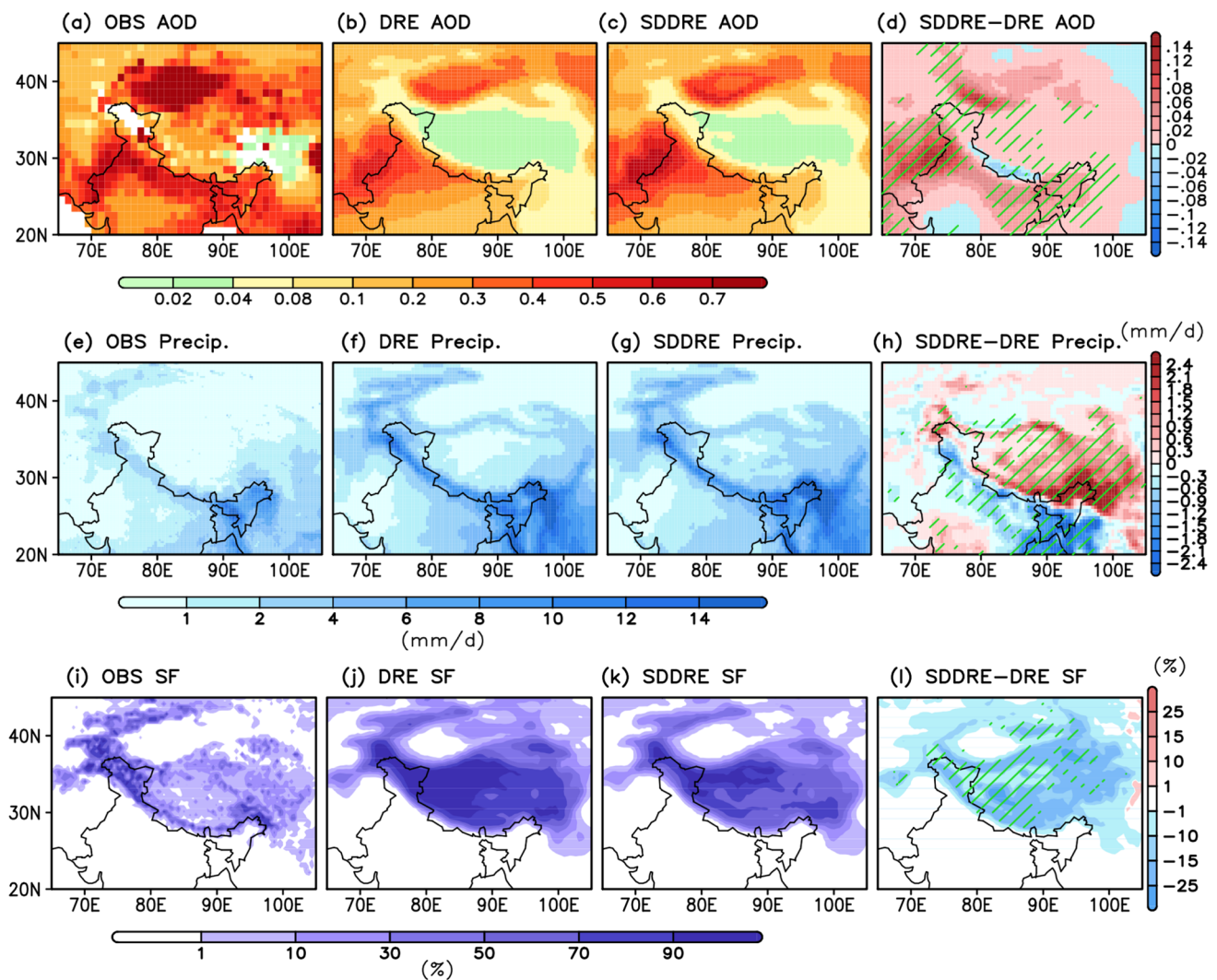


Fig. 3 Spatial distribution of AOD (top panel) from **a** MODIS, **b** DRE, **c** SDDRE, and **d** difference between SDDRE and DRE. Similar arrangements in the middle and bottom panel for precipitation (**e–h**) and snow fraction (**i–l**) except observations taken from TRMM for

precipitation and MODIS for snow fraction during the pre-monsoon (March to June) for the period 2006–2010. The green slant lines represent regions with 95% significance level

HTP in SDDRE, by 10 to 15%, which is a likely primary contributor to the reduced cold bias there (Figs. 31). The reduction of snow is mainly associated with mineral dust due to larger rates of deposition over the region compared to BC (Fig. 4a–b). Dust deposition is also found over the northern territories of the HTP, where there is little contribution from BC. The area-averaged dust deposition is higher in the western Himalayas ($\sim 0.86 \text{ g m}^{-2}$), followed by the central ($\sim 0.48 \text{ g m}^{-2}$) and eastern Himalayas ($\sim 0.24 \text{ g m}^{-2}$). Similar patterns are found in the case of BC, with greater deposition in the western ($\sim 0.73 \text{ mg m}^{-2}$) and central Himalayas ($\sim 0.58 \text{ mg m}^{-2}$, see Fig. 5a). Dust originates from the nearby sources of the Taklamakan Desert and Gobi Desert (Kang et al., 2016), with the prevailing westerly winds and topographical forcings leading to uplifting of dust and transport

over these regions (Xu et al., 2018). A recent study by Sarangi et al. (2020) demonstrated that large concentrations of transported dust contribute to a decrease in snow albedo over the high mountain region of HTP.

In addition, the forcing induced by dust is strong and covers larger areas over the HTP compared to BC (Fig. 4c–d). The values ($> 10\text{--}25 \text{ W m}^{-2}$) for dust forcing on snow are larger over the northern HTP, while the BC forcing ranges between ~ 1 and 10 W m^{-2} , mostly limited to the southern HTP (Fig. 4d). A contribution to the melting of snow over the southern and southeastern parts of the HTP may also derive from BC deposition, since here the anthropogenic BC emitted from the IGP is transported by winds and is pushed up the hilly regions to be eventually deposited on the snow surface. Quantitatively, the area-averaged dust

Fig. 4 Spatial distribution of deposition of **a** dust and **b** BC on the snow top layer and forcing induced over snow by **c** dust and **d** BC during the pre-monsoon (March to June) for the period 2006–2010. The green, blue, and magenta boxes represent the western, central, and eastern Himalayas

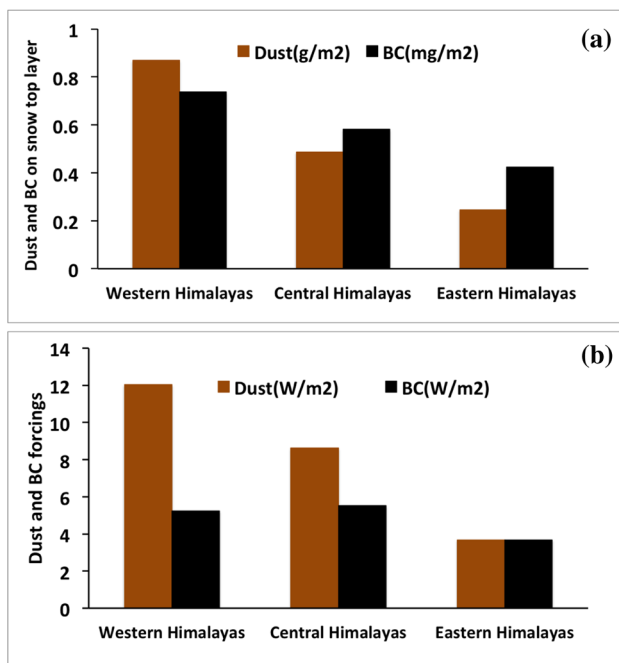
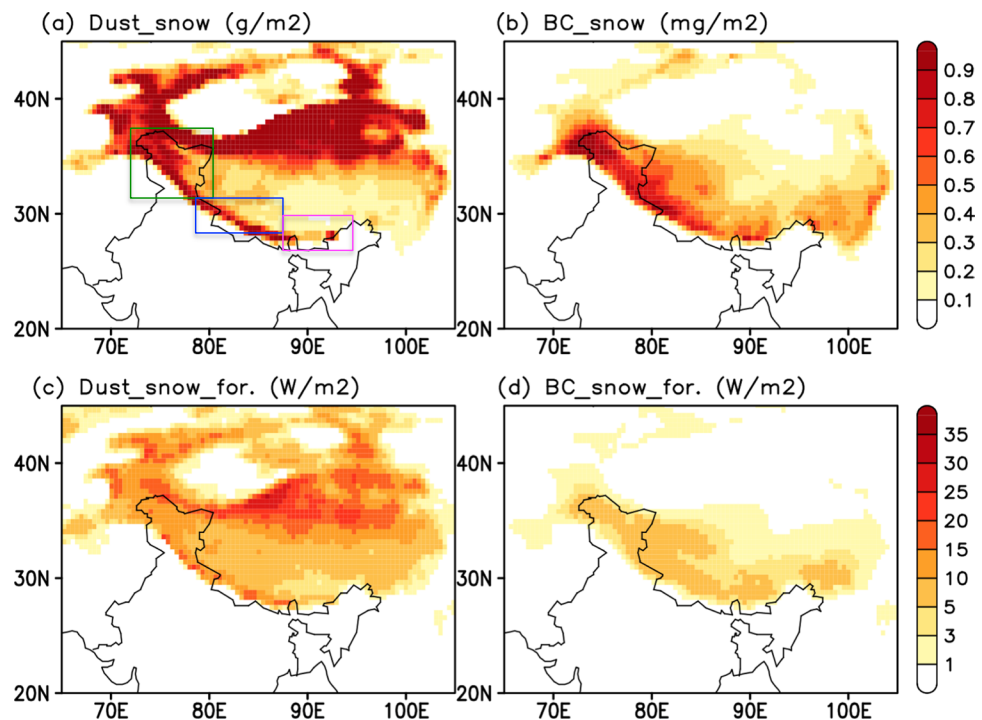


Fig. 5 **a** Dust (g/m²) and BC (mg/m²) mass deposition on the snow top layer and **b** dust- and BC aerosol-induced forcings (Wm⁻²) on snow over the western, central, and eastern Himalayas during the pre-monsoon (March to June) for the period 2006–2010

forcing is higher than 10 Wm⁻² over the western Himalayas compared to ~8 W m⁻² in the central and ~4 W m⁻² in the eastern Himalayas (Fig. 5b). The BC-induced forcing (~5 Wm⁻²) is similar in the western and central Himalayas, even

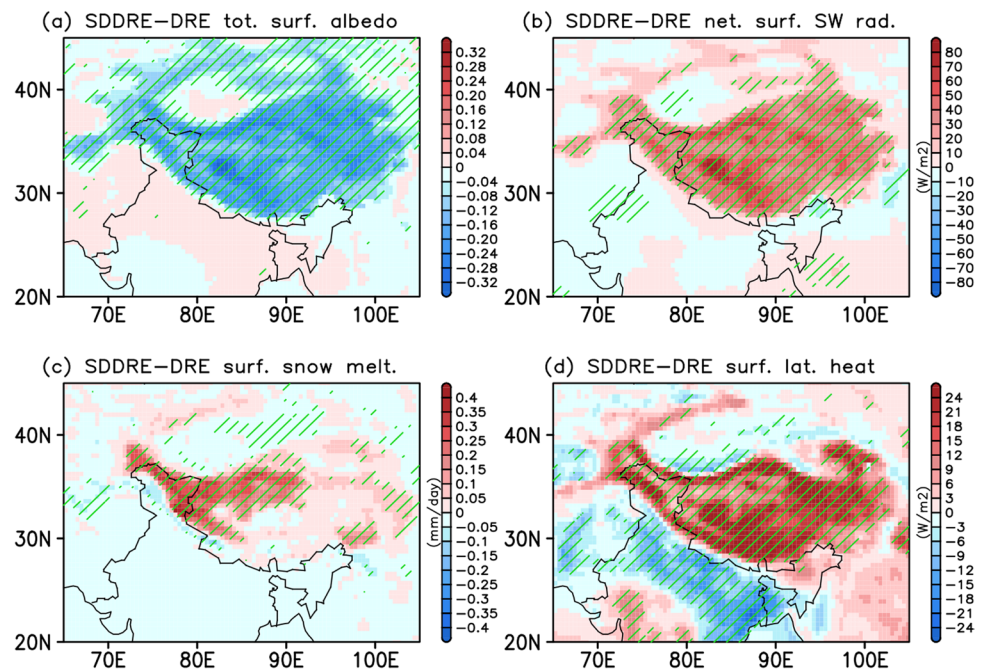
if the magnitude of BC deposition is slightly different over these regions. This is mainly due to the higher snow depth in the western Himalayas compared to the central Himalayas, which is considered for estimating the forcings. It is also interesting to note that the BC generates a forcing of similar magnitude as due by dust over the eastern Himalayas despite the lower BC deposition. This can be attributed to the more efficient light absorption by BC compared to dust (e.g., Usha et al., 2021).

3.2 Responses in northern India and HTP to aerosol-induced snow darkening effects

3.2.1 Thermal and dynamical responses

After the aerosol deposition on the snow top layer, the total surface albedo decreases by -0.24 to -0.32 over the HTP region (Fig. 6a), with maximum decrease (< -0.30) occurring in the northern and southern regions. This leads to increases in the absorption of incoming shortwave fluxes of more than 40 Wm⁻² (Fig. 6b). The associated increase in surface temperature (Fig. 2) enhances the snow melt over the HTP and in particular over its western portion, where a high snow fraction is simulated (Fig. 6c), thereby further enhancing the warming through the snow albedo feedback mechanism. The increase in the snow melt also contributes to a decrease in the total surface albedo by exposing the sub-surface layer (Lau and Kim 2018). As the snow melts, it contributes to an increase in latent heat flux (Fig. 6d), which acts as a moisture source for precipitation to occur over the

Fig. 6 Spatial distribution of mean anomalies due to aerosol-induced snow darkening effects in **a** total surface albedo, **b** surface shortwave radiation, **c** surface snow melt, and **d** surface upward latent heat during the pre-monsoon (March to June) seasons of the period 2006–2010. The green slant lines represent regions with 95% significance level



HTP. Apart from the increase in latent heat flux, the concomitant increase in sensible heat flux (Figure S2) over the HTP suggests the exposure of sub-surface darker layers (Das et al., 2020b).

As a result of the heat source over the HTP, there is an increase in the magnitude of surface winds coming from central and west Asia towards northern India, and aligning with the foothills (Fig. 7a). It is also seen that the southerly winds merge with the westerly flow over the IGP. Shi et al. (2018) found increases in northwest dry winds over India while investigating the effects of dust-induced snow darkening effects over the HTP. The increase in the wind intensity grows consistently in the vertical, up to 850 hPa, due to lower surface friction (Fig. 7c).

The changes in the vertical distribution of zonal wind (contours) and air temperature indicate strengthening of the zonal wind over the IGP along the Himalayan foothills (20–30° N) up to the middle of troposphere (~400 hPa; Fig. 8a). An interesting aspect of the snow darkening effect is the role of topography in advecting air mass from the plains to the HTP. For example, as the zonal winds strengthen, some air mass is lifted up along the topographic barrier imposed by the Himalayan foothills, which results in enhanced updrafts and precipitation there. This example highlights the importance of using high-resolution models over the region.

Apart from the changes in surface temperature, changes of temperature in the troposphere are also noted, which can modulate the circulation patterns in the upper atmosphere. Positive values (sinking motion) of vertical wind over northern India suggest suppression of convective activity

(Fig. 7d–f). This is mainly due to subsidence of dry air influx through the strengthened westerly winds. On the other hand, strong updrafts occur over the HTP due to surface heating (Fig. 8a), as also evident when looking at the changes in meridional circulations (Fig. 8b). The sinking circulation over the IGP (20–25° N) suggests an inhibition of convective updrafts over the region, which causes the precipitation decrease in SDDRE seen earlier. In addition, a decrease in specific humidity is related to the presence of dry air making the region drier and warmer. Conversely, negative vertical wind values (upward motion) are seen over the northern and southeastern part of the HTP, and the increase in specific humidity suggests the availability of moisture to form clouds and precipitate there.

As discussed earlier, the surface wind increases over the northwest regions of India, generating more dust from the Thar Desert to the IGP. In fact, we find a large increase in dust burden ($> 200 \text{ mg m}^{-2}$) over the Thar Desert, Taklamakan Desert, and IGP region in SDDRE compared to DRE (Fig. 9a), which can also be linked to lower precipitation there (Fig. 3g). This result is consistent with Xie et al. (2018). The increase in BC aerosol burden in SDDRE is limited mostly to the central and eastern Himalayas, but it is smaller in magnitude (~3 order) compared to dust (Fig. 9b). As a result of the snow darkening, precipitation decreases and there is an increase in sensible heat flux (> 9 to 15 W m^{-2}), which supports the formation of surface low-pressure anomalies over northern India (Figure S2) and the presence of dry and warm air over the region.

Clearly, the differences between the SDDRE and DRE simulations suggest a connection between the aerosol

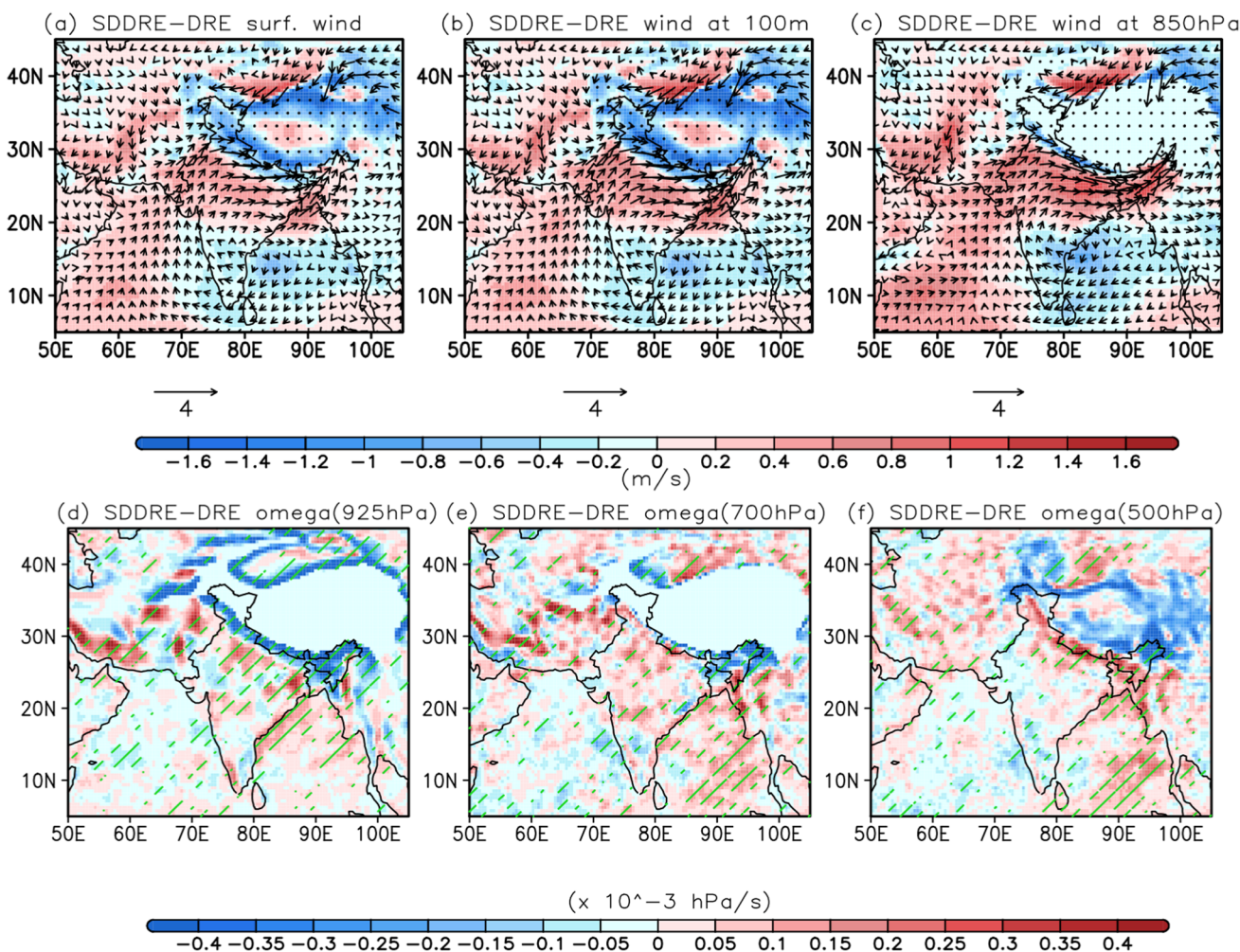


Fig. 7 Spatial distribution of mean anomalies induced in wind circulation (top panel) due to aerosol-induced snow darkening effects in **a** surface winds, **b** at 100 m, and **c** at 850 hPa. Bottom panel shows mean anomalies induced in omega at **d** 925 hPa, **e** 700 hPa, and

f 500 hPa during the pre-monsoon (March to June) for the period 2006–2010. The wind vectors and omega values are masked over the regions where topography exceeds 1500 m. The green slant lines represent regions with 95% significance level

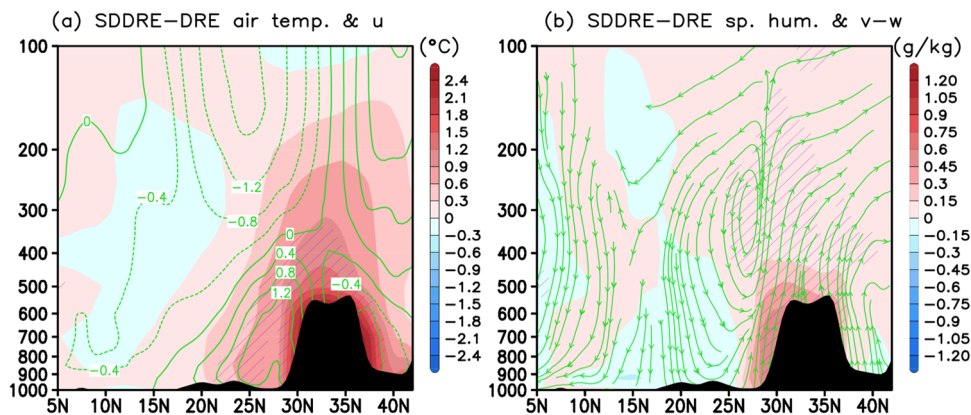


Fig. 8 Vertical cross-section averaged over longitudes (70–100°E) showing anomalies in **a** air temperature (shaded; units: °C), zonal winds (green contours; units: $m s^{-1}$) and **b** specific humidity (shaded; units: g/kg) and meridional circulations (green contours) due to aerosol-induced snow darkening effect during the pre-monsoon (March to

June) for the period 2006–2010. Omega is multiplied with the factor of 10^3 and both the plots are along 82° E longitude. The purple slant lines represent regions of significance at 95% level for the shaded variable

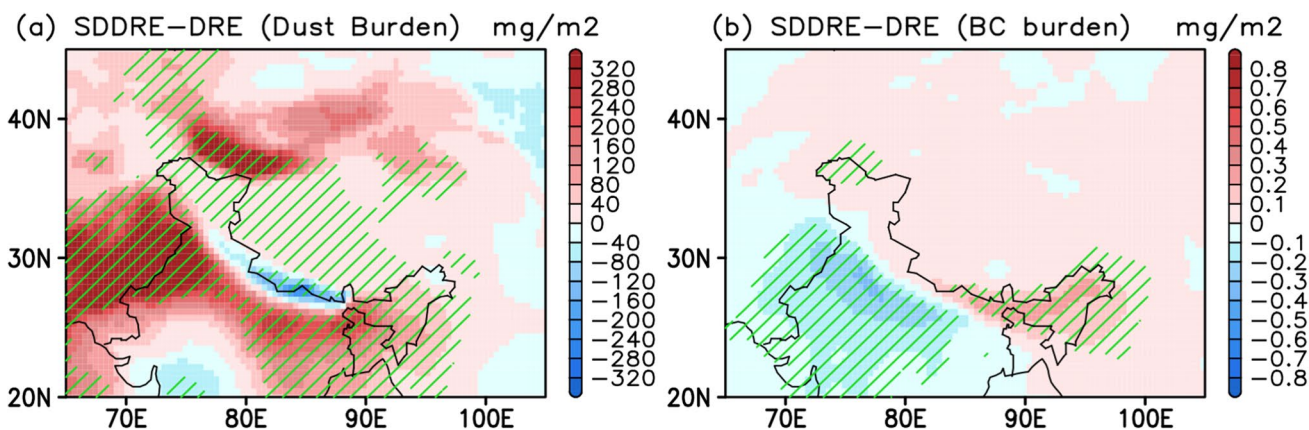


Fig. 9 Spatial distribution of mean anomalies in the aerosol species burden due to aerosol-induced snow darkening effects in **a** dust burden (mg m^{-2}) and **b** BC burden (mg m^{-2}) during the pre-monsoon

(March to June) for the period 2006–2010. The green slant lines represent regions with 95% significance level

deposition over the HTP and the dust cycle over northern India. Figure 10 shows the changes in dust emission and deposition caused by the snow darkening. The increase in dust emissions ($> 300 \text{ mg m}^{-2} \text{ day}^{-1}$) over the desert and semi-desert regions leads to increased dust burden in the SDDRE compared to the DRE case (Fig. 10a). The comparison of dry and wet deposition of dust shows that the former dominates over northern India, consistently with the decrease in precipitation there. Conversely, more wet deposition occurs over the HTP due to increased precipitation (Fig. 10b–c).

3.2.2 Response of meteorological extremes

We also investigated whether the snow darkening might affect daily precipitation and temperature indices such as the number of days when precipitation is greater than 1 mm/day,

10 mm/day (R10), and 20 mm/day (R20), the 95th percentile of precipitation (R95), the number of consecutive dry days (CDD), and the number of days when maximum temperature is above 40°C . Figure 11a shows that the mean number of days when the magnitude of precipitation events is greater than 1 mm/day decreases (less than 8–14 days) over the IGP, thus indicating lower intensity of precipitation associated with the drying found in SDDRE. Correspondingly, the number of consecutive dry days (~ 8 days) increases over northern India (Fig. 11b).

In terms of extreme precipitation indices, both R10 and R20 show a decrease in number of days (> 4 days) per season over most parts of northern India in SDDRE compared to DRE (Fig. 11d–e). Interestingly, there is an increase in heavy to very heavy precipitation days (> 7 days) over southeastern HTP, which may be a result of strong convective updrafts generated in SDDRE (Fig. 7f). The higher mean magnitude

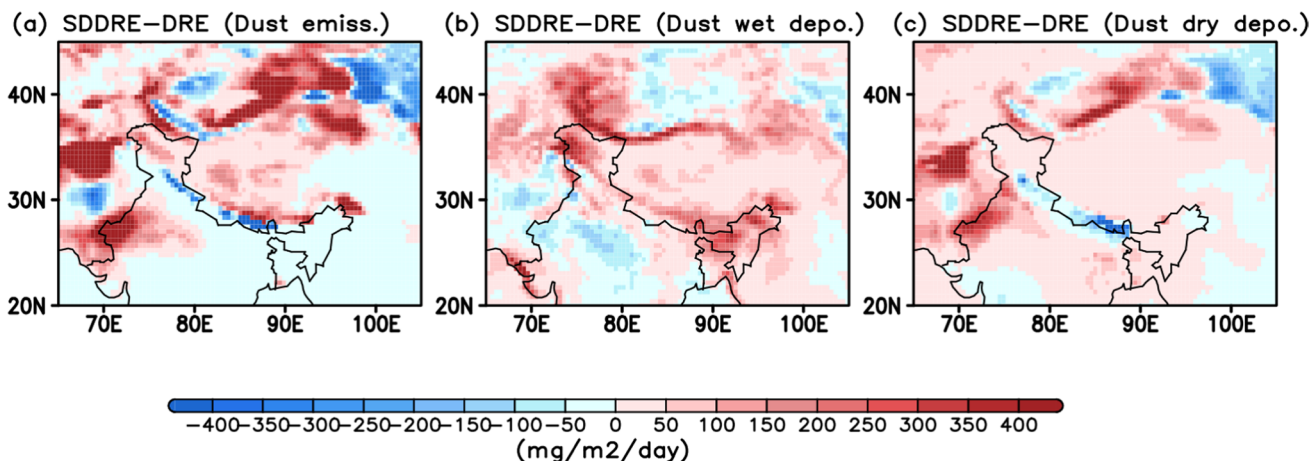


Fig. 10 Spatial distribution of mean anomalies due to aerosol-induced snow darkening effects in **a** dust emissions ($\text{mg m}^{-2} \text{ day}^{-1}$), **b** dust wet deposition ($\text{mg m}^{-2} \text{ day}^{-1}$), and **c** dust dry deposition ($\text{mg m}^{-2} \text{ day}^{-1}$) during the pre-monsoon (March to June) for the period 2006–2010

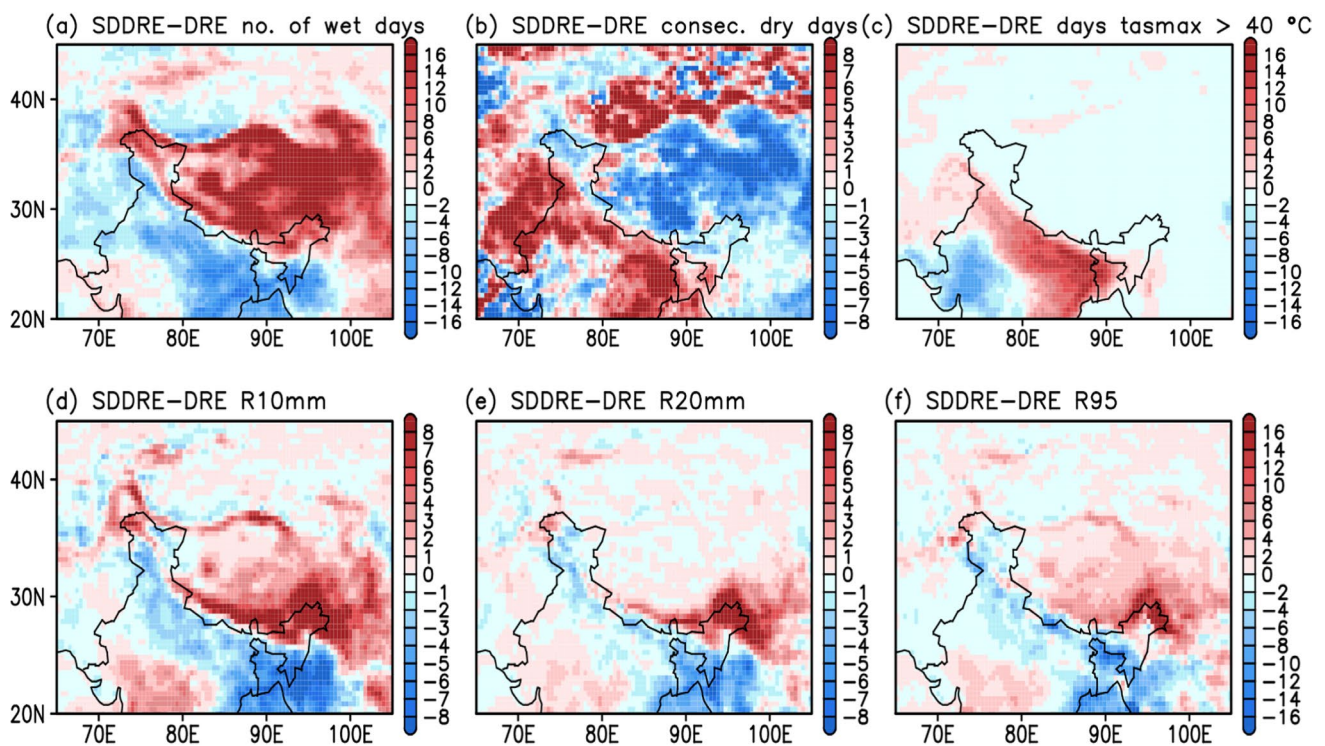


Fig. 11 Spatial distribution of mean anomalies due to aerosol-induced snow darkening effects in **a** number of wet days, **b** consecutive dry days, **c** number of days maximum temperature exceeding

40° C, **d** R10 days, **e** R20 days, and **f** R95 during the pre-monsoon (March to June) for the period 2006–2010

of R95 (> 4 mm/day) further supports the contribution of snow darkening in enhancing precipitation extremes over the eastern HTP (opposite to what happens in northern India).

One of the prerequisites to define high temperature extremes, e.g., leading to heat wave conditions, over northern India is for maximum temperature exceeding 40° C. Figure 11c shows that the number of days exceeding this threshold during the pre-monsoon increases by 8–14 days per season in SDDRE due to the temperature response to snow darkening. Therefore, our simulations suggest that over northern India, during the pre-monsoon season, the snow darkening leads to higher extreme temperatures, drier conditions, and reduced precipitation intensity and extremes along with increased dust burden.

3.2.3 Effects on monsoon onset

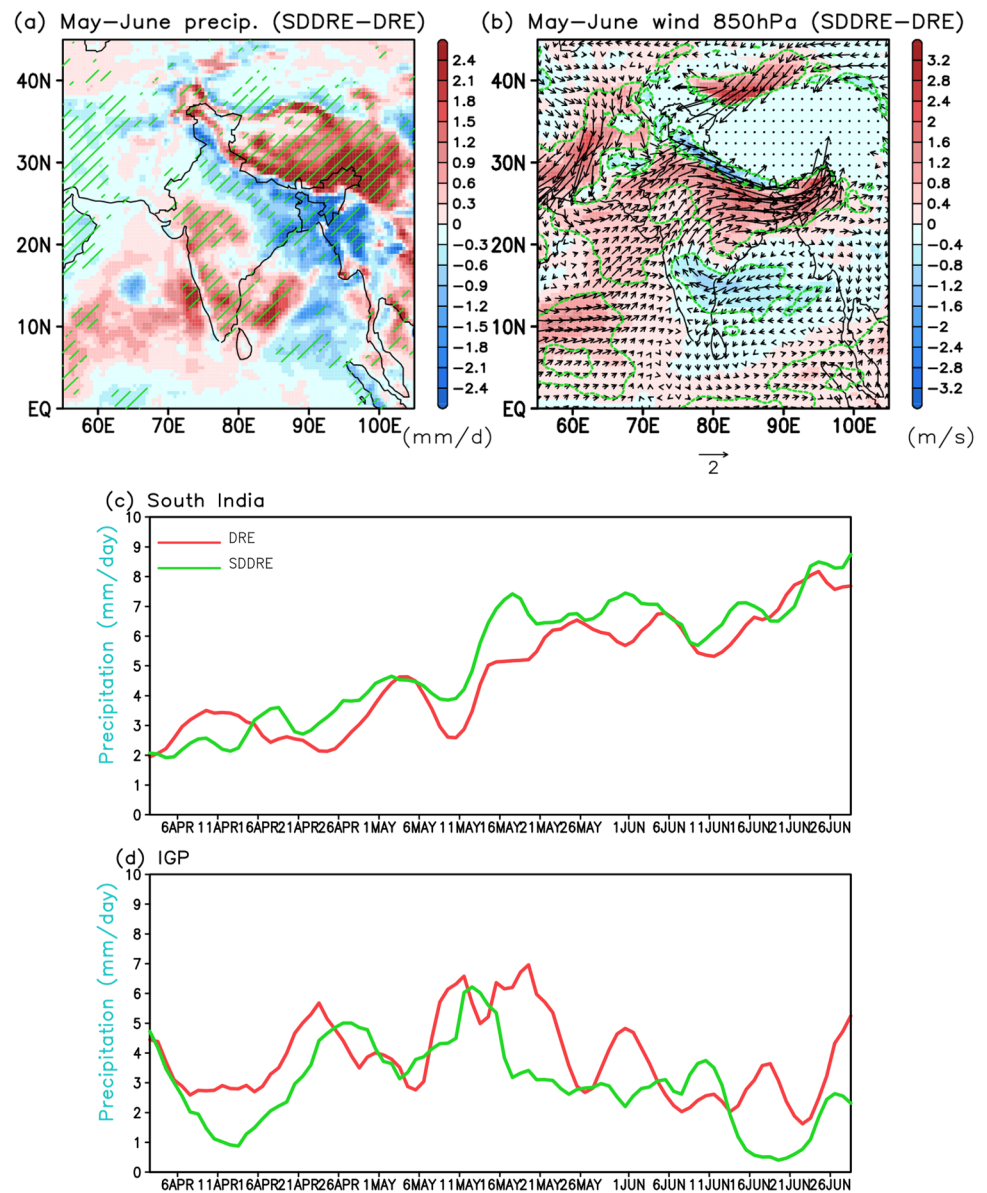
We examine now the possible link between aerosol effects (both DRE and SDDRE) and monsoon onset. For the monsoon onset analysis, we consider the months of May and June, during which the precipitation increase occurs mostly over the southern peninsula (> 1.5 mm/day) and extends up to parts of western India (Fig. 12a). In addition to the snow darkening feedback over the HTP, the buildup of elevated dust and BC aerosols along the Himalayan foothills and IGP

also heats up the atmospheric column. Here, the EHP mechanism drives the meridional thermal gradient, and enhances precipitation over the southern peninsula.

However, there is a decrease in precipitation over the IGP consistent with the changes seen during the whole pre-monsoon season. The strengthening of the northwest winds over the IGP causes a formation of an anticyclonic pattern over the Bay of Bengal centered over the eastern part of India (Fig. 12b). As a result, the northward propagation of southerly winds over the Indian mainland is reduced leading to a decrease in precipitation over northern India. At the same time, it is possible that the anticyclonic branch provides moisture from the Bay of Bengal towards south India, resulting in an increase in precipitation. The time series computed by taking a 5-day running mean over south India also show an increase in precipitation in SDDRE compared to DRE, whereas there is a decrease in precipitation over the IGP (Fig. 12c–d).

Following the methodology of Pradhan et al. (2017), we also use the climatological tropospheric temperature gradient (TTG) onset index for identifying the monsoon onset dates. First, we compute the tropospheric temperature gradient (ΔTT) by taking the difference of air temperature (averaged between 200 and 600 hPa) between a northern region defined by 30–110° E and 5–35° N and the

Fig. 12 Spatial distribution of mean anomalies due to aerosol-induced snow darkening effects in **a** precipitation and **b** wind circulations at 850 hPa during the during May–June for the period 2006–2010. Time series of 5-day running mean of area-averaged precipitation over the **c** south India and **d** Indo-Gangetic Plain in DRE and SDDRE during pre-monsoon. The winds are masked out over the HTP region. The green slant lines and contours represent regions with 95% significance level



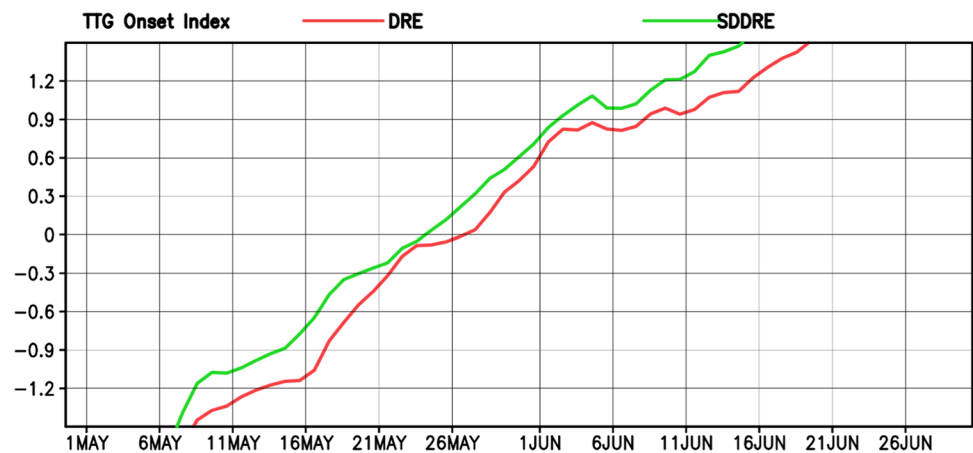
southern region $30\text{--}110^\circ\text{E}$ and $15^\circ\text{S}\text{--}5^\circ\text{N}$. The onset date is thus determined by the day in which the value of ΔTT changes sign from negative to positive.

The time series of climatological ΔTT is plotted in Fig. 13 for both the DRE and SDDRE experiments during May and June. We can see that the monsoon onset occurs earlier in the SDDRE by 1 to 3 days compared to DRE. This is the result of increased heating generated over the HTP region due to aerosol snow interactions (Figure S3), which builds up a larger temperature gradient (land-sea contrast). At the same time, even if there is an early arrival of the monsoon onset in SDDRE over south India, the northward propagation of precipitation is limited by the enhanced northwesterlies discussed earlier.

4 Summary and conclusions

The snow darkening effect by absorbing aerosols can have substantial impacts on the regional snow packs of the HTP and can cause snow and glacier melting, which can even exceed that induced by increasing greenhouse gases (e.g., Flanner et al., 2007, Flanner et al., 2009, Lau and Kim, 2018). This can lead to perturbations in the dynamics and thermodynamics of the atmosphere over the northern India region. To investigate this issue, in this paper, we carried out and intercompared two 5-year experiments, one with and one without aerosol snow darkening effects (SDDRE and DRE, respectively), using the RegCM4 regional

Fig. 13 Time series of climatological TTG onset index computed by taking difference between tropospheric air temperature between the northern (30–110° E, 5–35° N) and southern (30–110° E, 15°S–5°N) region for DRE and SDDRE experiments within the South Asia CORDEX domain during May–June for the period 2006–2010



climate model (Giorgi et al. 2012), coupled to an aerosol module (Solmon et al. 2006; Zakey et al. 2006, 2008) and focusing on the pre-monsoon season.

Our main conclusions can be summarized as follows:

1. The snow darkening effects caused by aerosol deposition tend to improve the simulation of mean and maximum temperature over the HTP. In particular, the cold biases in maximum temperature are highly reduced, by up to 4° C. The simulation of maximum temperature also improves over northern India, where the warming induced by snow darkening reaches 1–1.5° C, bringing temperatures closer to observations.
2. The snow pattern drastically improves in SDDRE, with a reduction of 10 to 15% of excess snow fractional cover. Larger deposition of dust compared to BC contributes to such snow reduction.
3. A dipole pattern in precipitation change is found as a response to snow darkening, with increases over the HTP (~0.8–1.6 mm/day) and decreases over northern India (~0.4–2.1 mm/day). The precipitation increase over the HTP is at least partially due to an increase in snowmelt, soil moisture, and latent heat flux, which provides moisture over the region. Precipitation biases over northern India are reduced by the inclusion of snow darkening.
4. The AOD simulation improves with the inclusion of snow darkening mostly over the dust source regions, i.e., the Thar Desert and Taklimakan desert, due to increased emissions caused by strengthening of winds. In response to strengthened winds and decreased precipitation, there are significant changes in the dust cycle over northern India. Strong surface heating leads to the formation of low surface pressure, which amplifies dust emissions over the desert sources and its transport along the IGP.
5. Overall, in northern India, the aerosol-induced snow darkening over the HTP leads to decrease in mean and extreme precipitation indices (i.e., number of precipita-

tion days > 1 mm/day, R10, R20) and increase in the number of consecutive dry days with very high temperatures and high dust burden.

6. Snow darkening induces an earlier monsoon onset by ~1–3 days over southern India due to higher tropospheric temperature gradients caused by the aerosol deposition over the HTP. However, the northward progression of precipitation is hindered by the enhanced northwesterly winds over IGP.

These results should be seen in view of a few caveats. First, the resolution of our current experiments (grid spacing 50 km), which was mostly determined by the availability of computer resources in relation to the expense of running the coupled aerosol module over such a large domain, may not be sufficient to resolve the HTP topography in fine detail. Very recent RegCM4 developments allow us to carry out convection permitting simulations at a few kilometer grid spacing (Coppola et al., 2020), and this may help us in better simulating topographically forced and convection processes. Second, our simulations are based on a simple aerosol module where only absorbing aerosol species are considered (dust and BC), as they are the primary snow darkening agents (Flanner et al., 2007). More aerosol species could however be included for a more comprehensive assessment of aerosol effects. Third, there is always an uncertainty in the anthropogenic aerosol inventories (Gadhavi et al., 2015) in terms of sources that are not accounted for (e.g., bio fuels, wildfires). We are currently conducting work in all these three directions in order to improve our simulation protocol.

Despite these issues, our study clearly indicates that the aerosol snow darkening effect has an important role in improving the model simulation over the HTP and northern India during the pre-monsoon season. This should also improve the simulation of the inception and development of the ISM, an issue worthy of further investigation in future studies. Our simulations are also suggestive of strong effects of the snow darkening on the dynamics and thermodynamics

of the region. Hence, it is recommended to consider the snow darkening effect by dust and carbonaceous aerosols over the South Asia region in future climate scenario simulations to investigate how this may vary under different greenhouse gas forcings.

Supplementary Information The online version contains supplementary material available at <https://doi.org/10.1007/s00704-021-03871-y>.

Acknowledgements We thank the anonymous reviewers for the constructive comments that improved the quality of the manuscript. The authors are thankful to the supercomputing facility provided by Marconi installed in CINECA machine and Argo at ICTP, where all the simulations and initial model tuning were carried out respectively. ICTP's RegCM4 model is freely available online in <https://github.com/ictp-esp/RegCM/releases>. The anthropogenic aerosol emissions considered for baseline and mitigation of SLCPs are taken from ECLIPSE data inventory.

The data can be accessed from an online website clicking the following link <http://www.iiasa.ac.at/web/home/research/researchPrograms/air/ECLIPSEv5a.html>. The lateral boundary conditions and topographical data can be downloaded from <http://clima-dods.ictp.it/data/regcm4/>. All the observation data sources are highly acknowledged. The first author is thankful to the UN-ICTP's postdoctoral fellowship for carrying out the research. A.S. Panicker and A.S. Gautam acknowledge ICTP, Italy, for Junior Associateship for collaborative research. VSN acknowledges SwarnaJayanti Fellowship of DST, Govt. of India.

Author contribution SD and FG conceptualized the research. SD, FG, and EC customized the RegCM model over the region of study. SD performed the model simulations with the inputs from EC, VSN, and GG. ASP and ASG helped in analyzing the model results. All the authors contributed in writing, analyzing, and finalizing the manuscript.

Data availability All the ICBC and anthropogenic aerosol emission data used to run the model are archived in <http://clima-dods.ictp.it/data/regcm4/>. The model simulated data can be made available from the corresponding author on reasonable request.

Code availability The RegCM model code can be downloaded from <https://github.com/ictp-esp/RegCM/releases>.

Declarations

Ethics approval All the authors comply with the guidelines of the journal Theoretical and Applied Climatology.

Consent to participate All the authors agreed to participate in this study.

Consent for publication All the authors agreed to the publication of this study.

Conflict of interest The authors declare no competing interests.

References

Ajay P, Pathak B, Solmon F et al (2019) Obtaining best parameterization scheme of RegCM 4.4 for aerosols and chemistry simulations

over the CORDEX South Asia. *Clim Dyn* 53:329–352. <https://doi.org/10.1007/s00382-018-4587-3>

Albrecht BA (1989) Aerosols, Cloud Microphysics, and Fractional Cloudiness. *Science* 245:1227–1230. <https://doi.org/10.1126/science.245.4923.1227>

Aloysius M, Sijikumar S, Prijith S et al (2011) Role of dynamics in the advection of aerosols over the Arabian Sea along the west coast of peninsular India during pre-monsoon season: A case study based on satellite data and regional climate model. *J Earth Syst Sci* 120:269–279. <https://doi.org/10.1007/s12040-011-0051-z>

Ashfaq M, Cavazos T, Reboita MS et al (2020) Robust late twenty-first century shift in the regional monsoons in RegCM-CORDEX simulations. *Clim Dyn*. <https://doi.org/10.1007/s00382-020-05306-2>

Bollasina MA, Ming Y, Ramaswamy V (2011) Anthropogenic aerosols and the weakening of the south asian summer monsoon. *Science* (80-) 334:502–505. <https://doi.org/10.1126/science.1204994>

Bond TC, Doherty SJ, Fahey DW et al (2013) Bounding the role of black carbon in the climate system: A scientific assessment. *J Geophys Res Atmos* 118:5380–5552. <https://doi.org/10.1002/jgrd.50171>

Coppola E, Sobolowski S, Pichelli E et al (2020) A first-of-its-kind multi-model convection permitting ensemble for investigating convective phenomena over Europe and the Mediterranean. *Clim Dyn* 55:3–34. <https://doi.org/10.1007/s00382-018-4521-8>

Chen X, Liu Y (2017) Wu, G (2017) Understanding the surface temperature cold bias in CMIP5 AGCMs over the Tibetan Plateau. *Adv Atmos Sci* 34:1447–1460. <https://doi.org/10.1007/s00376-017-6326-9>

Dagsson-Waldhauserova P, Meinander O (2019) Editorial: Atmosphere—Cryosphere Interaction in the Arctic, at High Latitudes and Mountains With Focus on Transport, Deposition, and Effects of Dust, Black Carbon, and Other Aerosols. *Front Earth Sci* 7:1–4. <https://doi.org/10.3389/feart.2019.00337>

Das S, Dey S, Dash SK, Basil G (2013) Examining mineral dust transport over the Indian subcontinent using the regional climate model, RegCM4.1. *Atmos Res* 134. doi: <https://doi.org/10.1016/j.atmosres.2013.07.019>

Das S, Dey S, Dash SK et al (2015) Dust aerosol feedback on the Indian summer monsoon: Sensitivity to absorption property. *J Geophys Res* 120. <https://doi.org/10.1002/2015JD023589>

Das S, Giorgi F, Giuliani G et al (2020a) Near-Future Anthropogenic Aerosol Emission Scenarios and Their Direct Radiative Effects on the Present-Day Characteristics of the Indian Summer Monsoon. *J Geophys Res Atmos* 125. <https://doi.org/10.1029/2019JD031414>

Das S, Giorgi F, Giuliani G (2020b) Investigating the relative responses of regional monsoon dynamics to snow darkening and direct radiative effects of dust and carbonaceous aerosols over the Indian subcontinent. *Clim Dyn* 55. <https://doi.org/10.1007/s00382-020-05307-1>

Dee DP, Uppala SM, Simmons AJ et al (2011) The ERA-Interim reanalysis: Configuration and performance of the data assimilation system. *Q J R Meteorol Soc* 137:553–597. <https://doi.org/10.1002/qj.828>

Dey S, Di Girolamo L (2010) A climatology of aerosol optical and microphysical properties over the Indian subcontinent from 9 years (2000–2008) of Multiangle Imaging Spectroradiometer (MISR) data. *J Geophys Res Atmos* 115:1–22. <https://doi.org/10.1029/2009JD013395>

Dey S, Tripathi SN, Singh RP, Holben BN (2004) Influence of dust storms on the aerosol optical properties over the Indo-Gangetic basin. *J Geophys Res D Atmos* 109:1–13. <https://doi.org/10.1029/2004JD004924>

Dumka UC, Kaskaoutis DG, Francis D, Chaboureaud JP, Rashki A, Tiwari S et al (2019) The role of the Intertropical Discontinuity region and the heat low in dust emission and transport over the Thar desert, India: A premonsoon case study. *Journal of*

- Geophysical Research: Atmospheres 124:13197–13219. <https://doi.org/10.1029/2019JD030836>
- Emanuel K, Zivkovic-Rothman M (2000) Comments on “Development and Evaluation of a Convection Scheme for Use in Climate Models.” *J Atmos Sci* 57:3686–3686. [https://doi.org/10.1175/15200469\(2000\)057%3c3686:codaao%3e2.0.co;2](https://doi.org/10.1175/15200469(2000)057%3c3686:codaao%3e2.0.co;2)
- Fan J, Wang Y, Rosenfeld D, Liu X (2016) Review of aerosol-cloud interactions: Mechanisms, significance, and challenges. *J Atmos Sci* 73:4221–4252. <https://doi.org/10.1175/JAS-D-16-0037.1>
- Flanner MG, Zender CS, Hess PG et al (2009) Springtime warming and reduced snow cover from carbonaceous particles. *Atmos Chem Phys* 9:2481–2497. <https://doi.org/10.5194/acp-9-2481-2009>
- Flanner MG, Zender CS, Randerson JT, Rasch PJ (2007) Present-day climate forcing and response from black carbon in snow. *J Geophys Res Atmos* 112:1–17. <https://doi.org/10.1029/2006JD008003>
- Gadhavi HS, Renuka K, Ravi Kiran V et al (2015) Evaluation of black carbon emission inventories using a Lagrangian dispersion model - A case study over southern India. *Atmos Chem Phys* 15:1447–1461. <https://doi.org/10.5194/acp-15-1447-2015>
- Giorgi F, Jones C, Asrar G (2009) Addressing climate information needs at the regional level: The CORDEX framework. *WMO Bulletin* 58:175–183
- Giorgi F, Coppola E, Solmon F et al (2012) RegCM4: Model description and preliminary tests over multiple CORDEX domains. *Clim Res* 52:7–29. <https://doi.org/10.3354/cr01018>
- Giorgi F, Bi X, Qian Y (2002) Direct radiative forcing and regional climatic effects of anthropogenic aerosols over East Asia: A regional coupled climate-chemistry/aerosol model study. *J Geophys Res Atmos* 107:AAC 7–1–AAC 7–18. doi: <https://doi.org/10.1029/2001JD001066>
- Giorgi F (2019) Thirty Years of Regional Climate Modeling: Where Are We and Where Are We Going next? *J Geophys Res Atmos* 124:5696–5723. <https://doi.org/10.1029/2018JD030094>
- Grenier H, Bretherton CS (2001) A moist PBL parameterization for large-scale models and its application to subtropical cloud-topped marine boundary layers. *Mon Weather Rev* 129:357–377. [https://doi.org/10.1175/1520-0493\(2001\)129%3c0357:AMPPFL%3e2.0.CO;2](https://doi.org/10.1175/1520-0493(2001)129%3c0357:AMPPFL%3e2.0.CO;2)
- Guo L, Turner AG, Highwood EJ (2016) Local and remote impacts of aerosol species on Indian summer monsoon rainfall in a GCM. *J Clim* 29:6937–6955. <https://doi.org/10.1175/JCLI-D-15-0728.1>
- Hall DK, Riggs GA (2007) Assessment of Errors in the MODIS Suite of Snow-Cover Products. *Hyrol Process* 21:1534–1547
- Harris I, Osborn TJ, Jones P, Lister D (2020) Version 4 of the CRU TS monthly high-resolution gridded multivariate climate dataset. *Sci Data* 7:1–18. <https://doi.org/10.1038/s41597-020-0453-3>
- He C, Takano Y, Liou KN et al (2017) Impact of snow grain shape and black carbon-snow internal mixing on snow optical properties: Parameterizations for climate models. *J Clim* 30:10019–10036. <https://doi.org/10.1175/JCLI-D-17-0300.1>
- He C, Flanner MG, Chen F et al (2018) Black carbon-induced snow albedo reduction over the Tibetan Plateau: Uncertainties from snow grain shape and aerosol-snow mixing state based on an updated SNICAR model. *Atmos Chem Phys* 18:11507–11527. <https://doi.org/10.5194/acp-18-11507-2018>
- Hu Z, Huang J, Zhao C et al (2020) Modeling dust sources, transport, and radiative effects at different altitudes over the Tibetan Plateau. *Atmos Chem Phys* 20:1507–1529. <https://doi.org/10.5194/acp-20-1507-2020>
- Huffman GJ, Adler RF, Bolvin DT, Nelkin EJ (2010) The TRMM Multi-Satellite Precipitation Analysis (TMPA) In: Satellite rainfall applications for surface hydrology. *Satell. Rainfall Appl. Surf. Hydrol.*, 1–327. <https://doi.org/10.1007/978-90-481-2915-7>
- Ji Z, Kang S, Cong Z et al (2015) Simulation of carbonaceous aerosols over the Third Pole and adjacent regions: distribution, transportation, deposition, and climatic effects. *Clim Dyn* 45:2831–2846. <https://doi.org/10.1007/s00382-015-2509-1>
- Kang L, Huang J, Chen S, Wang X (2016) Long-term trends of dust events over Tibetan Plateau during 1961–2010. *Atmos Environ* 125:188–198. <https://doi.org/10.1016/j.atmosenv.2015.10.085>
- Kiehl JT, Hack JJ, Bonan GB, et al (1996) Description of the NCAR Community Climate Model (CCM3). NCAR Tech Note NCAR/TN-420+STR 159
- Kumar R, Barth MC, Pfister GG et al (2014) WRF-Chem simulations of a typical pre-monsoon dust storm in northern India: Influences on aerosol optical properties and radiation budget. *Atmos Chem Phys* 14:2431–2446. <https://doi.org/10.5194/acp-14-2431-2014>
- Lau KM, Kim KM (2006) Observational relationships between aerosol and Asian monsoon rainfall, and circulation. *Geophys Res Lett* 33:1–5. <https://doi.org/10.1029/2006GL027546>
- Lau KM, Kim MK, Kim KM (2006) Asian summer monsoon anomalies induced by aerosol direct forcing: The role of the Tibetan Plateau. *Clim Dyn* 26:855–864. <https://doi.org/10.1007/s00382-006-0114-z>
- Lau WKM, Kim KM (2018) Impact of snow darkening by deposition of light-absorbing aerosols on snow cover in the Himalayas-Tibetan Plateau and influence on the Asian summer monsoon: A possible mechanism for the blanford hypothesis. *Atmosphere (basel)* 9. <https://doi.org/10.3390/atmos9110438>
- Lee WL, Liou KN, He C et al (2017) Impact of absorbing aerosol deposition on snow albedo reduction over the southern Tibetan plateau based on satellite observations. *Theor Appl Climatol* 129:1373–1382. <https://doi.org/10.1007/s00704-016-1860-4>
- Levy RC, Mattoo S, Munchak LA et al (2013) The Collection 6 MODIS aerosol products over land and ocean. *Atmos Meas Tech* 6:2989–3034. <https://doi.org/10.5194/amt-6-2989-2013>
- Liu Z (2015) Evaluation of precipitation climatology derived from TRMM multi-satellite precipitation analysis (TMPA) monthly product over land with two gauge-based products. *Climate* 3:964–982. <https://doi.org/10.3390/cli3040964>
- Li Z, Lau WKM, Ramanathan V et al (2016) Aerosol and monsoon climate interactions over Asia. *Rev Geophys* 54:866–929. <https://doi.org/10.1002/2015RG000500>
- Maharana P, Dimri AP, Choudhary A (2019) Redistribution of Indian summer monsoon by dust aerosol forcing. *Meteorol Appl* 26:584–596. <https://doi.org/10.1002/met.1786>
- Ming J, Wang P, Zhao S, Chen P (2013) Disturbance of light-absorbing aerosols on the albedo in a winter snowpack of Central Tibet. *J Environ Sci (China)* 25:1601–1607. [https://doi.org/10.1016/S1001-0742\(12\)60220-4](https://doi.org/10.1016/S1001-0742(12)60220-4)
- Nair VS, Solmon F, Giorgi F et al (2012) Simulation of South Asian aerosols for regional climate studies. *J Geophys Res Atmos* 117:1–17. <https://doi.org/10.1029/2011JD016711>
- Ojha N et al (2020) On the widespread enhancement in fine particulate matter across the Indo-Gangetic Plain towards winter. *Sci Rep* 10:1–9. <https://doi.org/10.1038/s41598-020-62710-8>
- Oleson KW, Lawrence DM, Bonan GB, et al (2013) CLM 4.5 NCAR Technical Note. NCAR Tech Note
- Pal JS, Small EE, Eltahir EAB (2000) Simulation of regional-scale water and energy budgets: Representation of subgrid cloud and precipitation processes within RegCM. *J Geophys Res Atmos* 105:29579–29594. <https://doi.org/10.1029/2000JD900415>
- Panicker AS, Pandithurai G, Dipu S (2010) Aerosol indirect effect during successive contrasting monsoon seasons over Indian subcontinent using MODIS data. *Atmos Environ* 44:1937–1943. <https://doi.org/10.1016/j.atmosenv.2010.02.015>
- Pattayak KC, Panda SK, Saraswat V, Dash SK (2016) Relationship between tropospheric temperature and Indian summer monsoon rainfall as simulated by RegCM3. *Clim Dyn* 46:3149–3162. <https://doi.org/10.1007/s00382-015-2758-z>

- Pradhan M, Rao AS, Srivastava A, Dakate A, Salunke K, Shameera KS (2017) Prediction of Indian Summer-Monsoon Onset Variability: A Season in Advance. *Sci Rep* 7:1–14. <https://doi.org/10.1038/s41598-017-12594-y>
- Qian Y, Flanner MG, Leung LR, Wang W (2011) Sensitivity studies on the impacts of Tibetan Plateau snowpack pollution on the Asian hydrological cycle and monsoon climate. *Atmos Chem Phys* 11:1929–1948. <https://doi.org/10.5194/acp-11-1929-2011>
- Ramanathan V, et al (2005) Atmospheric brown clouds: Impacts on South Asian climate and hydrological cycle. *Proc Natl Acad Sci U S A* 102:5326–5333. <https://doi.org/10.1073/pnas.0500656102>
- Rana A, Nikulin G, Kjellström E et al (2020) Contrasting regional and global climate simulations over South Asia. *Clim Dyn* 54:2883–2901. <https://doi.org/10.1007/s00382-020-05146-0>
- Sanjay J, Krishnan R, Shrestha AB et al (2017) Downscaled climate change projections for the Hindu Kush Himalayan region using CORDEX South Asia regional climate models. *Adv Clim Chang Res* 8:185–198. <https://doi.org/10.1016/j.accre.2017.08.003>
- Saranghi C, Qian Y, Rittger K et al (2018) Impact of light-absorbing particles on snow albedo darkening and associated radiative forcing over High Mountain Asia: High resolution WRF-Chem modeling and new satellite observations. *Atmos Chem Phys Discuss* 1–56. <https://doi.org/10.5194/acp-2018-979>
- Saranghi C, Qian Y, Rittger K, Leung LR, Chand D, Bormann KJ, Painter TH (2020) Dust dominates high-altitude snow darkening and melt over high-mountain Asia. *Nat Clim Chang* 10:1045–1105. <https://doi.org/10.1038/s41558-020-00909-3>
- Sarkar S, Chauhan A, Kumar R, Singh RP (2019) Impact of Deadly Dust Storms (May 2018) on Air Quality, Meteorological, and Atmospheric Parameters Over the Northern Parts of India. *GeoHealth* 3:67–80. <https://doi.org/10.1029/2018gh000170>
- Schmale J, Flanner M, Kang S et al (2017) Modulation of snow reflectance and snowmelt from Central Asian glaciers by anthropogenic black carbon. *Sci Rep* 7:1–10. <https://doi.org/10.1038/srep40501>
- Sharma D, Singh D, Kaskaoutis DG (2012) Impact of two intense dust storms on aerosol characteristics and radiative forcing over Patiala. *Northwestern India Adv Meteorol* 2012. <https://doi.org/10.1155/2012/956814>
- Shi Z, Xie X, Li X et al (2018) Snow-darkening versus direct radiative effects of mineral dust aerosol on the Indian summer monsoon: role of the Tibetan Plateau. *Atmos Chem Phys Discuss* 1–29. <https://doi.org/10.5194/acp-2018-471>
- Solmon F, Giorgi F, Liou C (2006) Aerosol modelling for regional climate studies: Application to anthropogenic particles and evaluation over a European/African domain. *Tellus, Ser B Chem Phys Meteorol* 58:51–72. <https://doi.org/10.1111/j.1600-0889.2005.00155.x>
- Srivastava AK, Tiwari S, Devara PCS et al (2011) Pre-monsoon aerosol characteristics over the Indo-Gangetic Basin: Implications to climatic impact. *Ann Geophys* 29:789–804. <https://doi.org/10.5194/angeo-29-789-2011>
- Stohl A, Aamaas B, Amann M et al (2015) Evaluating the climate and air quality impacts of short-lived pollutants. *Atmos Chem Phys* 15:10529–10566. <https://doi.org/10.5194/acp-15-10529-2015>
- Swenson SC, Lawrence DM (2012) A new fractional snow-covered area parameterization for the Community Land Model and its effect on the surface energy balance. *J Geophys Res* 117:D21107. <https://doi.org/10.1029/2012JD018178>
- Tiedtke M (1989) A Comprehensive Mass Flux Scheme for Cumulus Parameterization in Large-Scale Models. *Mon Weather Rev* 117:1779–1800
- Tiwari PR, Kar SC, Mohanty UC et al (2016) On the dynamical downscaling and bias correction of seasonal-scale winter precipitation predictions over North India. *Q J R Meteorol Soc* 142:2398–2410. <https://doi.org/10.1002/qj.2832>
- Twomey S (1974) Pollution and the planetary albedo. *Atmos Environ* 8:1251–1256
- Usha KH, Nair VS, Babu SS (2020) Modeling of aerosol induced snow albedo feedbacks over the Himalayas and its implications on regional climate. *Clim Dyn* 54:4191–4210. <https://doi.org/10.1007/s00382-020-05222-5>
- Usha KH, Nair VS, Babu SS, (2021) Effect of aerosol-induced snow darkening on the direct radiative effect of aerosols over the Himalayan region. *Environ. Res. Lett* (accepted).
- Wang C (2013) Impact of anthropogenic absorbing aerosols on clouds and precipitation: A review of recent progresses. *Atmos Res* 122:237–249. <https://doi.org/10.1016/j.atmosres.2012.11.005>
- Xie X, Liu X, Che H et al (2018) Radiative feedbacks of dust in snow over eastern Asia in CAM4-BAM. *Atmos Chem Phys* 18:12683–12698. <https://doi.org/10.5194/acp-18-12683-2018>
- Xu C, Ma Y, Yang K, You C (2018) Tibetan Plateau impacts on global dust transport in the upper troposphere. *J Clim* 31:4745–4756. <https://doi.org/10.1175/JCLI-D-17-0313.1>
- Yasunari TJ, Tan Q, Lau KM et al (2014) Estimated range of black carbon dry deposition and the related snow albedo reduction over Himalayan glaciers during dry pre-monsoon periods. *Atmos Environ* 78:259–267. <https://doi.org/10.1016/j.atmosenv.2012.03.031>
- Zakey AS, Solmon F, Giorgi F (2006) Development and testing of a desert dust module in a regional climate model. *Atmos Chem Phys Discuss* 6:1749–1792. <https://doi.org/10.5194/acpd-6-1749-2006>
- Zakey AS, Giorgi F, Bi X (2008) Modeling of sea salt in a regional climate model: Fluxes and radiative forcing. *J Geophys Res Atmos* 113:1–27. <https://doi.org/10.1029/2007JD009209>
- Zender CS, Bian H, Newman D (2003) Mineral Dust Entrainment and Deposition (DEAD) model: Description and 1990s dust climatology. *J Geophys Res Atmos* 108. <https://doi.org/10.1029/2002jd002775>
- Zhang R, Wang H, Qian Y et al (2015) Quantifying sources, transport, deposition, and radiative forcing of black carbon over the Himalayas and Tibetan Plateau. *Atmos Chem Phys* 15:6205–6223. <https://doi.org/10.5194/acp-15-6205-2015>

Publisher's note Springer Nature remains neutral with regard to jurisdictional claims in published maps and institutional affiliations.